3. EXPERIMENTAL APPARATUS

3.1 Wind Tunnel

The experiments were conducted using a low speed wind tunnel. The schematic diagram and the whole view of the experimental facility are shown in Figs. 3.1 and 3.2, respectively. The wind tunnel consists of a driving section, rectification section, and test section. Low turbulence flow entering the test section was insured by conditioning the flow in the rectification section which was placed upstream of the test section. The wind tunnel was driven by an electric blower (model SFJ-304-IV-I). The flow leaving the blower entered a chamber with screens and a honeycomb. From the diffuser, the flow entered the honeycomb, passed through two fine-meshed screens, and entered the nozzle. The blower insured that the flow rate was steady and that the freestream velocity varied from 0 to 13 m/s with a freestream turbulence intensity of $\pm$ 1.5 percent. The test section inlet dimensions were 250×120 mm (W $\times$ H). The test section had the function of variable diffuser which could adjust the divergence angle α between 0 and 45 degrees. A detailed diagram of the test section is shown in Fig. 3.2. The jet flow was delivered through a needle valve and an electric valve (model 2AF5-10) after accumulating the air into a tank by using a compressor. A rotameter (model J-2693) was placed at the downstream of the metering valve. The magnitude of the jet flow rate was characterized by the jet-to-freestream velocity ratio VR ($=V_j / U_0$). Figure 3.3 shows the configuration of jets and the coordinate system used to describe the flow field. The origins of coordinate X, Y, and Z were defined as the location of the jet orifice, the lower wall, and the left wall of the test section (viewed from upstream), respectively. Three jet orifices were placed at the upstream of the

divergent lower wall and were configured on the right-hand side of the lower wall in the test section (viewed from upstream). The jets were skewed with respect to the freestream direction (0 degrees being downstream) and were pitched to the lower wall. The jet skew angle and the pitch angle were denoted as θ and ϕ, respectively. In this study, the jet skew angle was set at 90 degrees (θ=90 degrees). The jet pitch angle and the jet orifice diameter could be changed by replacing the jet orifice unit shown in Fig. 3.4.

3.2 Laboratory Computer

Data acquisition and experiment control were accomplished using a SORD SRV4100-500 computer with an i486DX4 processor and had 20 MB of memory. The system included four interface boards connected to the ISA-Bus and VL-Bus which were used to sample the data and control the experimental instruments. The interface boards were a digital-to-analog converter (D/A), an analog-to-digital converter (A/D), and a stepping motor control unit. Both the A/D and D/A converters had 12-bit resolution. The A/D converter was utilized in the hot wire data and the differential pressure data acquisition. The D/A converter was utilized in the control of an electric valve.

3.3 Velocity Measurement Instruments

3.3.1 X-Array Hot Wire [39, 40]

The velocity field was measured using an X-array hot wire probe. A schematic of the X-array probe is shown in Fig. 3.5. This probe consists of two constant temperature anemometer sensors positioned nominally at 45 degrees to the streamwise direction and 90 degrees to

each other. The probe was a Model 0252R-T5 with two tungsten wires 5 μm in diameter and four support needles. The probe tip was rotated into the *U-V*, *U-W* planes in order to obtain three-dimensional velocity. Each of the two wires was connected to a Model 1010 Constant Temperature Anemometer bridge operating with an overheat ratio of 1.5.

A calibration technique used to find the calibration curves of output voltage versus velocity was performed by setting the probe into a freestream. The velocity response was determined for nine velocities and a modified King's law was used to express the relationship between the fluid velocity and the output voltage of a hot wire anemometer. With an inclined hot wire the magnitude of the convection heat transfer from the wire is less than that with a hot wire set vertically in the flow, because the effective velocity component which has a relation to the convection heat transfer decreases. To understand how a heated sensor can be used to detect the angle between the hot wire sensor and the velocity vector, the velocity vector is separated into two components, a component normal to the wire and a component parallel to the wire. Although, both pass over the wire, the normal component is mainly responsible for sensor cooling. In other words, for a hot wire inclined at (π /2+ θ) degrees in the flow (see Fig. 3.6) the flow component along a hot wire can be assumed to be negligible and as a result the effective cooling velocity V_{eff} is written as

$$V_{eff} = v\cos\theta \qquad (3.1)$$

where v is the magnitude of the velocity vector and θ is defined as the angle between the velocity vector and the component normal to the wire. This relationship (3.1) is called the cosine law of a hot wire. The radiation heat transfer rate from the sensor to the surroundings is usually neglected, because the radiation heat loss is much lower than losses by convection to the fluid or conduction to the support needles for most applications. For a hot wire anemometer, King's law is usually written as

$$E^2 = a + bV_{eff}^n$$

(3.2)

where E is the anemometer output voltage, V_{eff} is the effective cooling velocity, and a, b, and n are King's law constants determined through a least squares fit.

The mean velocity components, U and V, were measured by setting a hot wire in the U-V plane (see Fig. 3.7(a)). Measurements in the U-W plane were used to obtain the mean velocity components W after a hot wire probe was rotated at 90 degrees around the probe axis (see Fig. 3.7(b)). For the case shown in Fig. 3.7(a), from Eq. (3.1) and Fig. 3.7(c) the effective cooling velocity of each hot wire is written as

$$\left.\begin{aligned} V_{effa1}^2 &= (v\cos\theta_1)^2 = v_{a2}^2 + W^2, \\ V_{effa2}^2 &= (v\cos\theta_2)^2 = v_{a1}^2 + W^2, \end{aligned}\right\} \tag{3.3}$$

where V_{effa1} and V_{effa2} indicate the effective cooling velocity of the No.1 hot wire and the No.2 hot wire, respectively. Furthermore, v_{a1} and v_{a2} indicate the velocity component along the No.1 and No.2 hot wire of Fig. 3.7(a) or 3.7(c), respectively. The mean velocity components, U and V, become

$$\left.\begin{aligned} U &= (v_{a1} + v_{a2})\cos 45°, \\ V &= (v_{a1} - v_{a2})\cos 45°. \end{aligned}\right\} \tag{3.4}$$

Therefore, v_{a1} and v_{a2} are written as

$$\left.\begin{aligned} v_{a1} &= \frac{U - V}{\sqrt{2}}, \\ v_{a2} &= \frac{U + V}{\sqrt{2}}. \end{aligned}\right\}$$

(3.5)

Substituting Eq. (3.5) into Eq. (3.3) we obtain the relationship between the effective cooling velocity and the mean velocity components, U, V and W:

$$\left.\begin{aligned} V_{effa1}^2 &= \frac{(U+V)^2}{2} + W^2, \\ V_{effa2}^2 &= \frac{(U-V)^2}{2} + W^2. \end{aligned}\right\} \tag{3.6}$$

Thus

$$V_{effa1} = \sqrt{\frac{(U+V)^2}{2} + W^2} = \frac{U}{\sqrt{2}}\sqrt{\left(1+\frac{V}{U}\right)^2 + 2\left(\frac{W}{U}\right)^2}$$

(3.7)

Hence, if the mean velocity components, V and W, are very small compared with the component U, we must have

$$\left(\frac{V}{U}\right)^2, \left(\frac{W}{U}\right)^2 \to 0$$

(3.8)

Taking Eq. (3.8) into account, we can obtain in the following modified form:

$$V_{effa1} = \frac{U}{\sqrt{2}}\sqrt{1+2\frac{V}{U}} = \frac{U}{\sqrt{2}}\left(1+\frac{V}{U}\right) = \frac{U+V}{\sqrt{2}}$$

(3.9)

and similarly we obtain

$$V_{effa2} = \frac{U-V}{\sqrt{2}}$$

(3.10)

Finally, for the configuration of two hot wires in Fig. 3.7(a), the relationship between the mean velocity components and the effective cooling velocity is described as follows:

$$\left.\begin{aligned} U &= \frac{1}{\sqrt{2}}(V_{effa1} + V_{effa2}), \\ V &= \frac{1}{\sqrt{2}}(V_{effa1} - V_{effa2}). \end{aligned}\right\}$$

(3.11)

For the configuration of two hot wires in Fig. 3.7(b), Eq. (3.3) is modified in the following form:

$$\left.\begin{aligned} V_{effb1}^2 &= v_{b2}^2 + V^2, \\ V_{effb2}^2 &= v_{b1}^2 + V^2. \end{aligned}\right\}$$

(3.12)

Thus

$$\left.\begin{aligned} U &= \frac{1}{\sqrt{2}}(V_{effb1} + V_{effb2}), \\ W &= \frac{1}{\sqrt{2}}(V_{effb1} - V_{effb2}). \end{aligned}\right\}$$

(3.13)

3.3.2 Streamwise Vorticity

It is necessary to know an accurate vorticity field in order to understand the structure of the vortices and to compute their strength. In this study, secondary velocity measurements were carried out to determine the streamwise vorticity at each data point. The streamwise vorticity is given as

$$\omega_x = \left(\frac{\partial W}{\partial Y} - \frac{\partial V}{\partial Z}\right)$$

(3.14)

The two terms on the right-hand side in Eq. (3.14) are discretized in space using second-order central finite-difference approximation. W_{n+1} or W_{n-1} is written, by using the Taylor series around the point a_n (see Fig. 3.8), as

$$W_{n+1} = W(Y + \Delta Y) = W_n + \Delta Y W_n' + \frac{1}{2}(\Delta Y)^2 W_n'' + \Lambda \quad ,$$

(3.15)

$$W_{n-1} = W(Y - \Delta Y) = W_n - \Delta Y W_n' + \frac{1}{2}(\Delta Y)^2 W_n'' - \Lambda \quad ,$$

(3.16)

hence each term of Eq. (3.14) can be written as

$$\frac{\partial W}{\partial Y} = W_n' \approx \frac{W_{n+1} - W_{n-1}}{2\Delta Y} \quad ,$$

(3.17)

and

$$\frac{\partial V}{\partial Z} = V_n' \approx \frac{V_{n+1} - V_{n-1}}{2\Delta Z} \quad ,$$

(3.18)

where ΔY and ΔZ denote a uniform mesh spacing in the normal direction and the spanwise direction, respectively. One-side difference is used at the boundary in the computational domain and $W_{n\pm2}$ or $W_{n\pm1}$ is written, by using the Taylor series around the point a_n (see Fig. 3.9), as

$$W_{n\pm2} = W_n \pm 2\Delta Y W_n' + \frac{(\pm 2\Delta Y)^2}{2!} W_n'' + \frac{(\pm 2\Delta Y)^3}{3!} W_n''' + \Lambda \quad ,$$

(3.19)

$$W_{n\pm1} = W_n \pm \Delta Y W_n' + \frac{(\pm \Delta Y)^2}{2!} W_n'' + \frac{(\pm \Delta Y)^3}{3!} W_n''' + \Lambda \quad ,$$

(3.20)

hence each term of Eq. (3.14) at the boundary region can be written as

$$\frac{\partial W}{\partial Y} = W_n' \approx \frac{-3W_n + 4W_{n+1} - W_{n+2}}{2\Delta Y} \qquad \text{(forward-difference),}$$

(3.21)

$$\frac{\partial W}{\partial Y} = W_n' \approx \frac{+3W_n - 4W_{n-1} + W_{n-2}}{2\Delta Y} \qquad \text{(backward-difference),}$$

(3.22)

and

$$\frac{\partial V}{\partial Z} = V_n' \approx \frac{-3V_n + 4V_{n+1} - V_{n+2}}{2\Delta Z} \qquad \text{(forward-difference),}$$

(3.23)

$$\frac{\partial V}{\partial Z} = V_n' \approx \frac{+3V_n - 4V_{n-1} + V_{n-2}}{2\Delta Z} \qquad \text{(backward-difference).}$$

(3.24)

3.3.3 Single-Wire Probe

Figure 3.10 indicates a single-wire probe which is used in order to measure the streamwise mean velocity in the boundary layer. The single-wire probe was DANTEC Model 9055P0141, which had a single-wire sensor attached to the tips of two support needles, and was

calibrated in the freestream near a Pitot tube which was used to measure the freestream velocity of the wind tunnel. The relationship between the output voltage of the single-wire probe and the fluid velocity was determined by using a linearizer Model 1013. The probe had a tip of a tungsten wire 5 μm in diameter. The single-wire was fixed vertically to the freestream.

3.3.4 Hot Wire Anemometer [39, 40]

The Wheatstone bridge is used in many electronic instruments to give an error signal proportional to the difference between a variable signal and a reference signal. Its use in hot wire anemometry is a typical application. The constant temperature anemometer uses a feedback amplifier to automatically maintain the sensor temperature constant. For constant temperature operation the adjustable resistor is set to a higher value than that for a balanced bridge based on the resistance of the unheated probe to prevent the oscillation of the circuit. The bridge voltage is increased to heat the sensor. This increases the sensor resistance and brings the bridge into balance. Any bridge imbalance caused by velocity variations is removed by readjusting the bridge voltage. The resulting bridge voltage is related to the fluid velocity through King's law.

3.3.5 Temperature Measurement Unit

Hot wire measurements required continuous temperature monitoring to make temperature corrections. The freestream temperature measurements for correcting temperature drift were made using a Model 1020 temperature measurement unit and probe. The probe sensor element is glass-plated platinum protected with a stainless steel pipe (see Fig. 3.11).

3.3.6 Three-Axis Automatic Probe Traversing Unit

Probe placement was achieved using a traversing mechanism that provided for automatic streamwise *X*, spanwise *Z*, and normal *Y* positioning and manual probe rotation about an axis parallel to the streamwise direction. Stepping motors (model KP6M2-005), stepping motor drivers (model SMD-301), and a stepping motor control unit (model SMC-3(PC)) were used to control the probe positioning. By using this method it was possible to control the probe placement at intervals of 0.1 mm in each direction.

3.4 Vortex Generator Jet Device

The vortex generator jet device is shown in Fig. 3.12. It consists of an electric motor (model M6100-201K) and a rotor disk. There is a hole 10 mm in diameter drilled into the rotor disk. The vortex generator can select steady flow or the pulsed flow jets. Pulsed flow was produced by passing or shutting off the secondary air from a compressor using the rotor which was driven by the electric motor. Steady jet flow was maintained if the rotor kept up the position passing the secondary air freely. In this study, the rotor allowed a pulse rate of up to 23 Hz. The revolutions per minute were measured with a revolution indicator (model 00204) which did not contact with the rotor.

3.5 Pressure Measurement Instruments

Static pressure measurements were made using a differential

pressure transducer Model 3051CD which was very sensitive to pressure difference (0.01 mmAq). The pressure value was converted from the output voltage of the differential pressure transducer by a linear calibration fit. Static pressure measurements in the test section were carried out at wall mounted static pressure taps in the downstream (see Fig. 3.13).

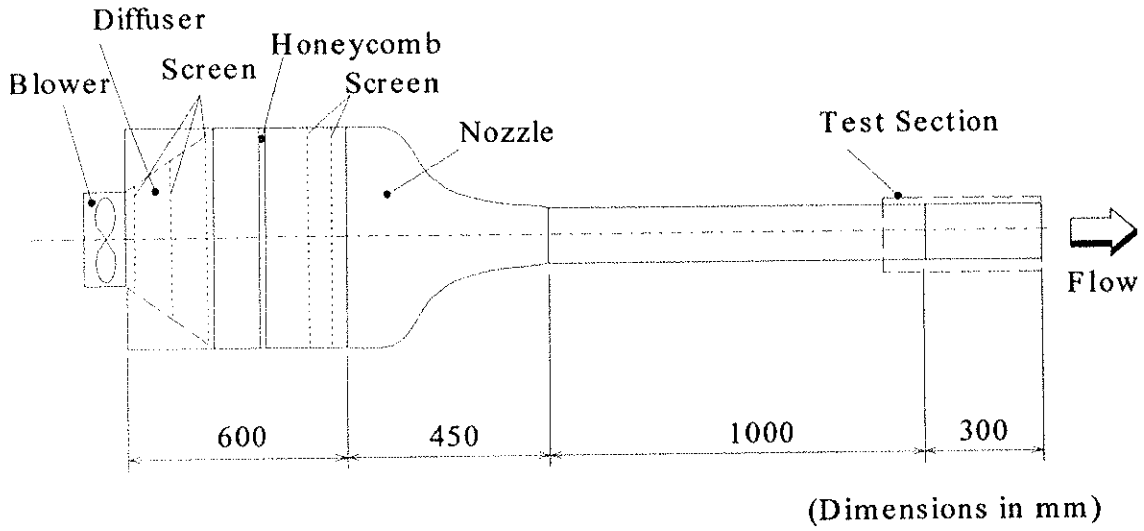

Figure 3.1 Schematic diagram of experimental facility.

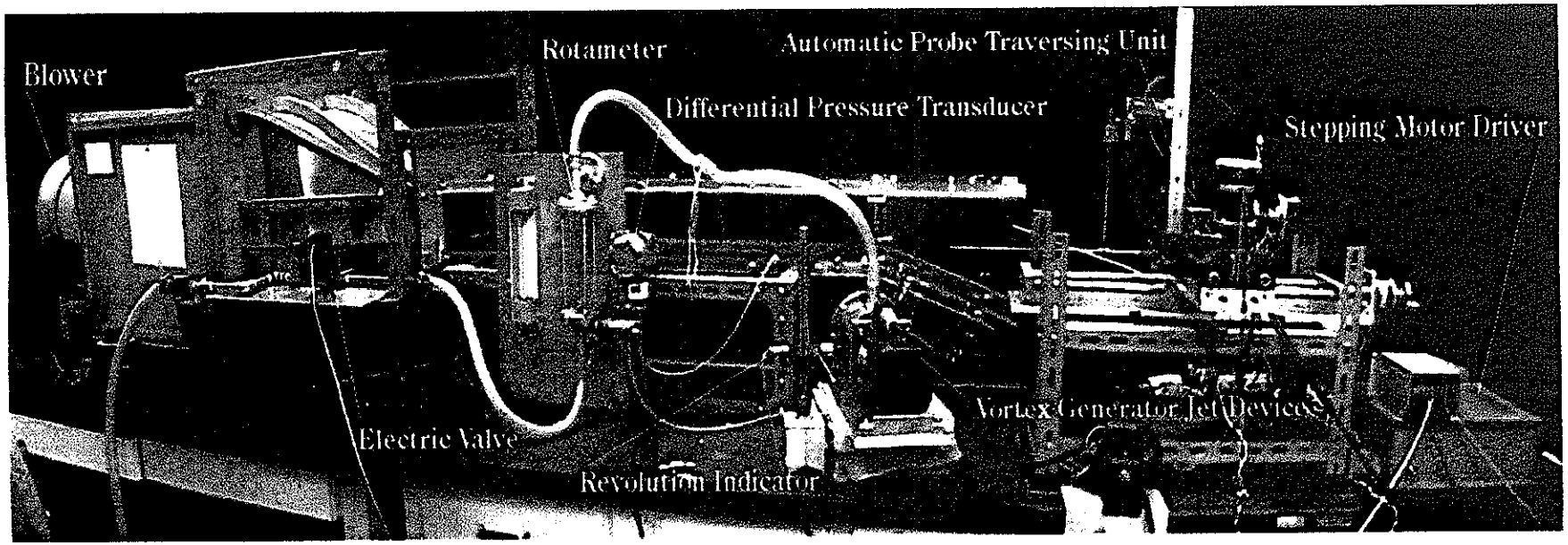

Figure 3.2 Whole view of experimental facility.

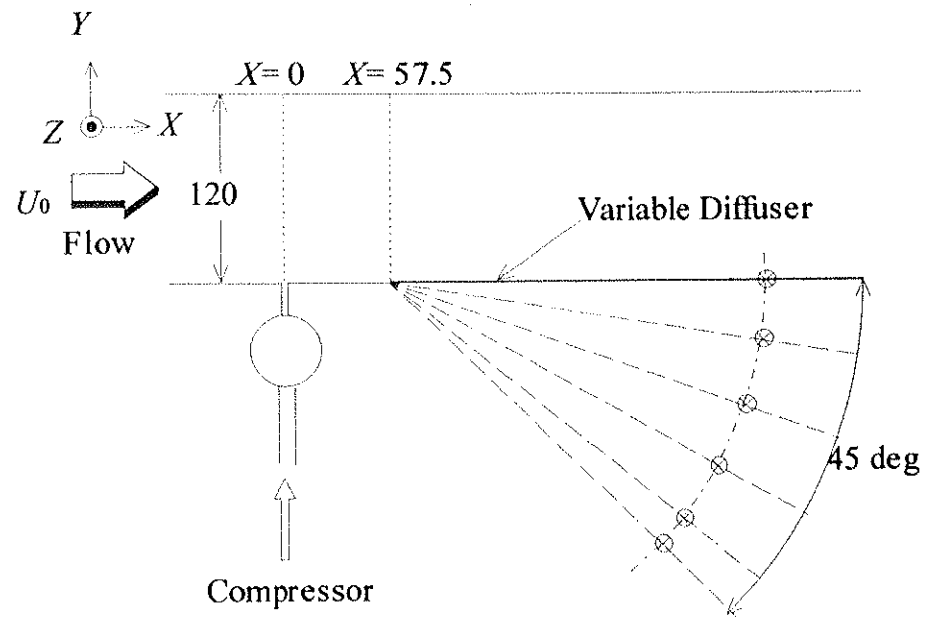

(Dimensions in mm)

Figure 3.3 Test section geometry.

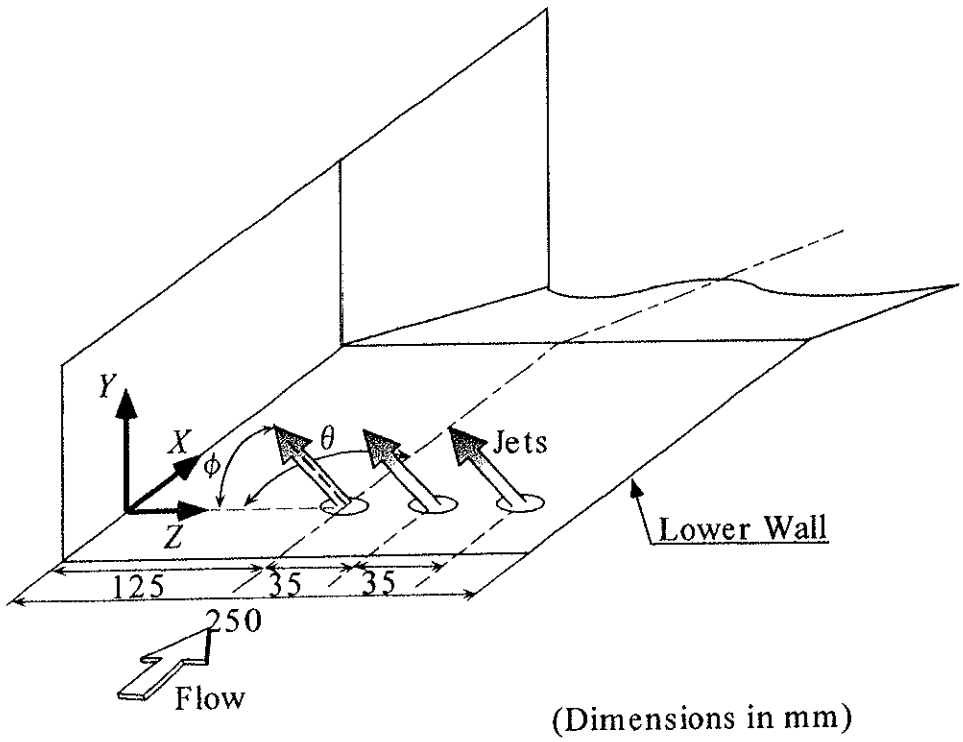

(Dimensions in mm)

Figure 3.4 Jet configurations in test section.

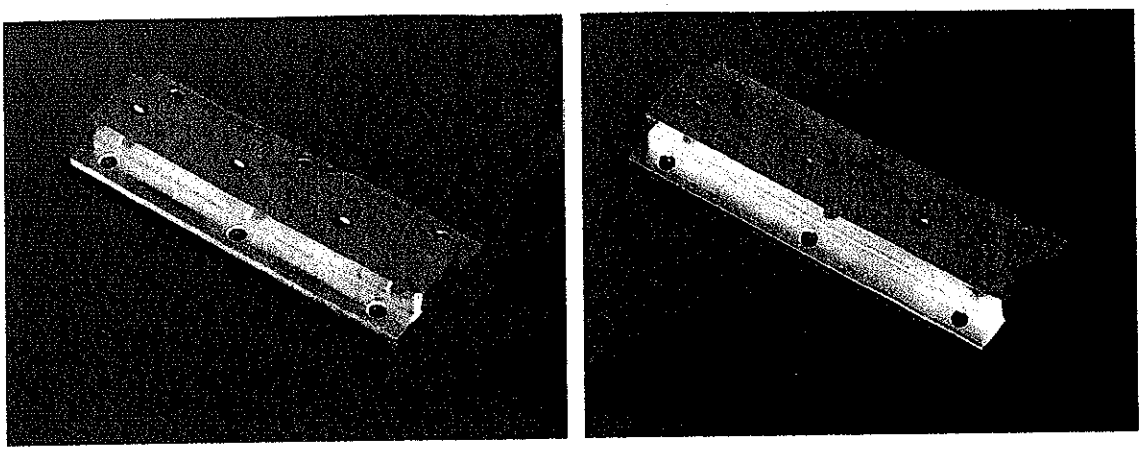

(a) D_f=2 mm, ϕ =30 deg

(b) D_f=2 mm, ϕ =45 deg

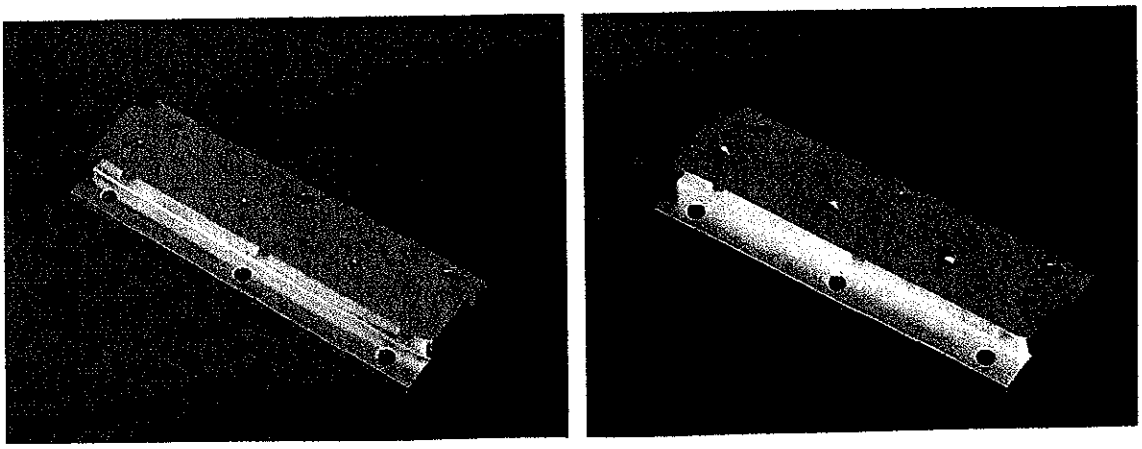

(c) D_f=2 mm, ϕ =60 deg

(d) D_f=3 mm, ϕ =45 deg

Figure 3.5 Jet orifice units.

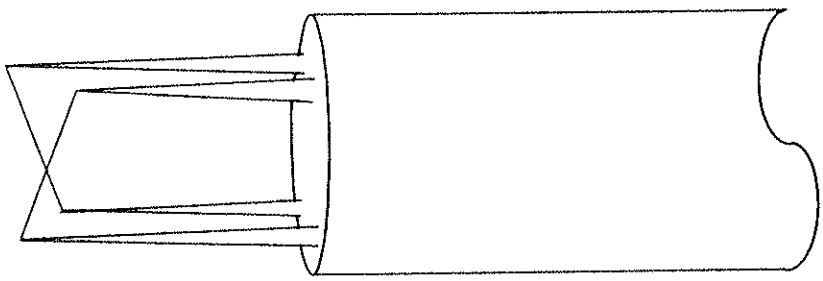

Figure 3.6 X-array hot wire probe.

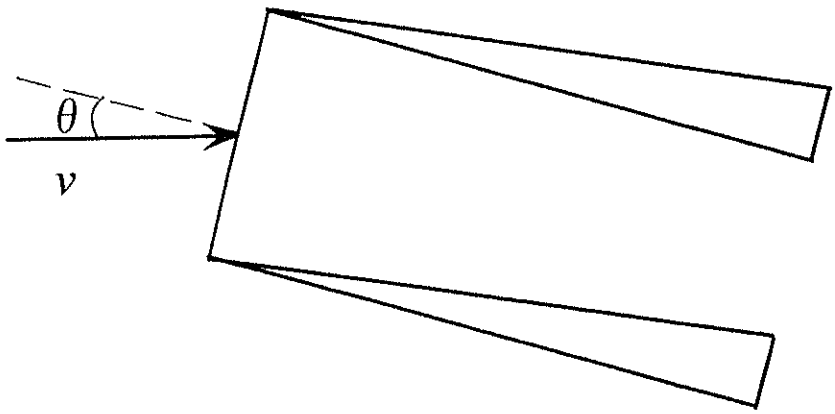

Figure 3.7 Inclined hot wire.

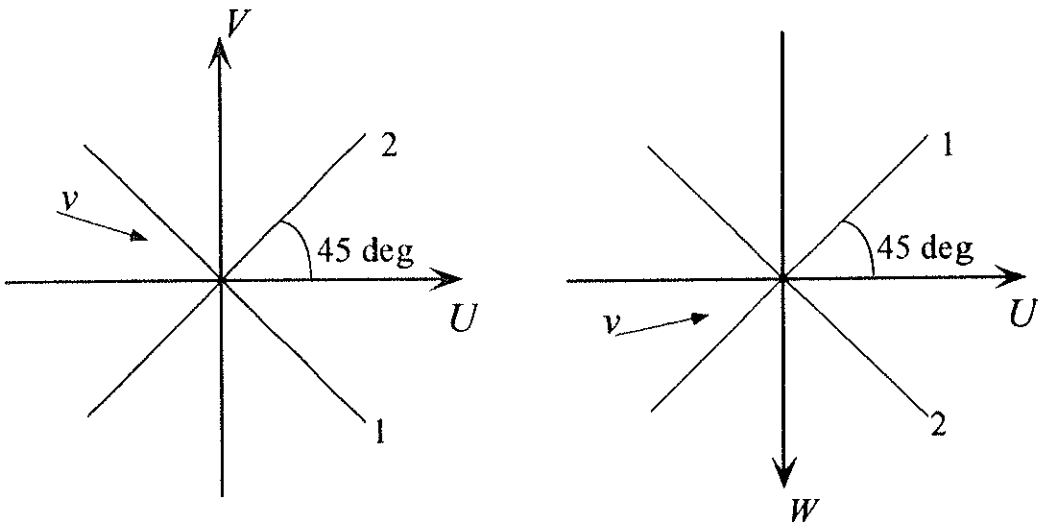

(a) *U-V* plane

(b) *U-W* plane

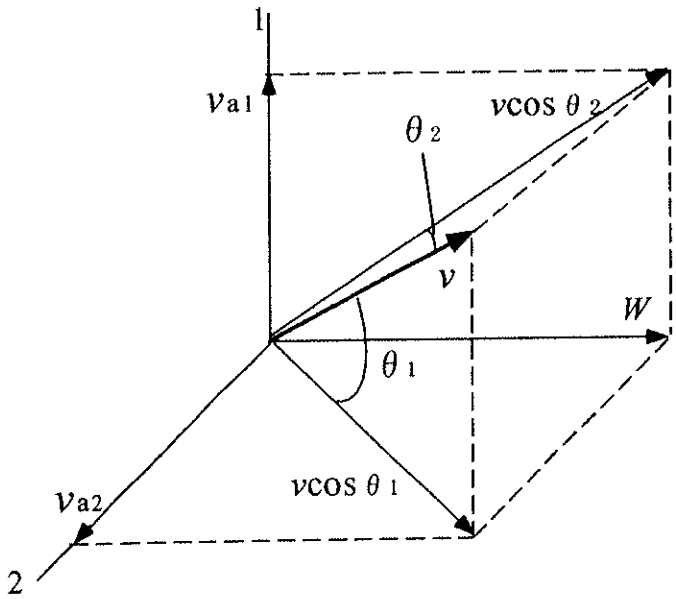

(c) No.1 or No.2 hot wire and velocity vector v

Figure 3.8 Hot wire configuration.

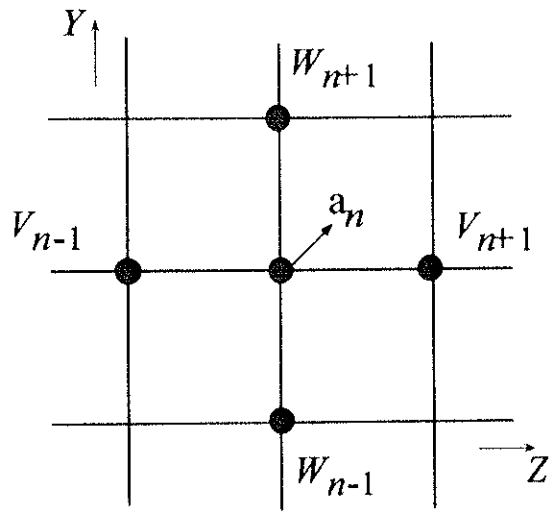

Figure 3.9 Inside of computational domain.

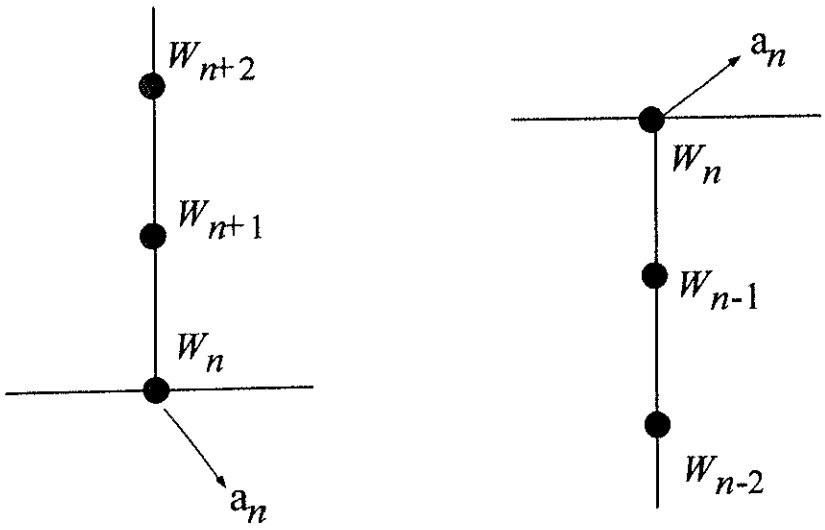

Figure 3.10 Boundary of computational domain.

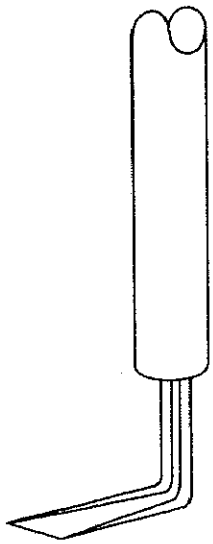

Figure 3.11 Single-wire probe.

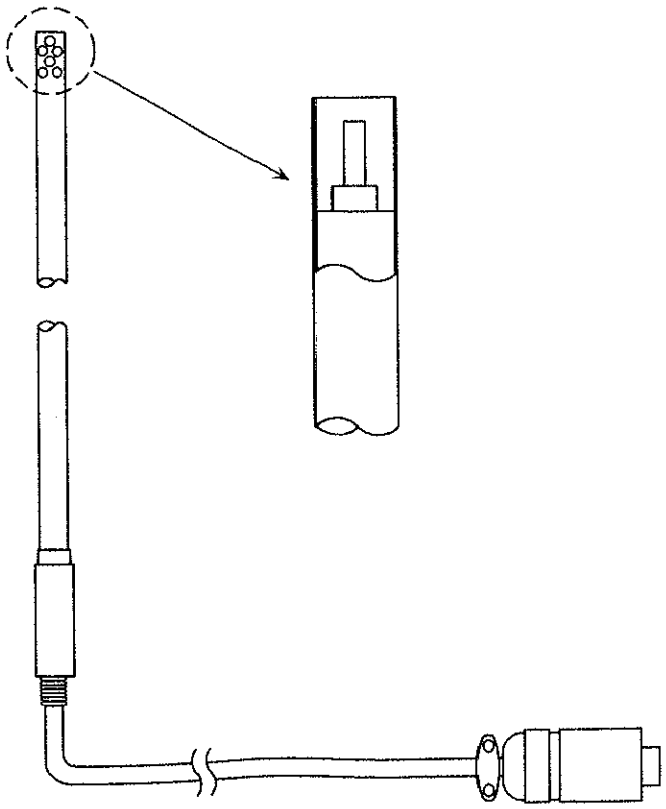

Figure 3.12 Temperature measurement probe.

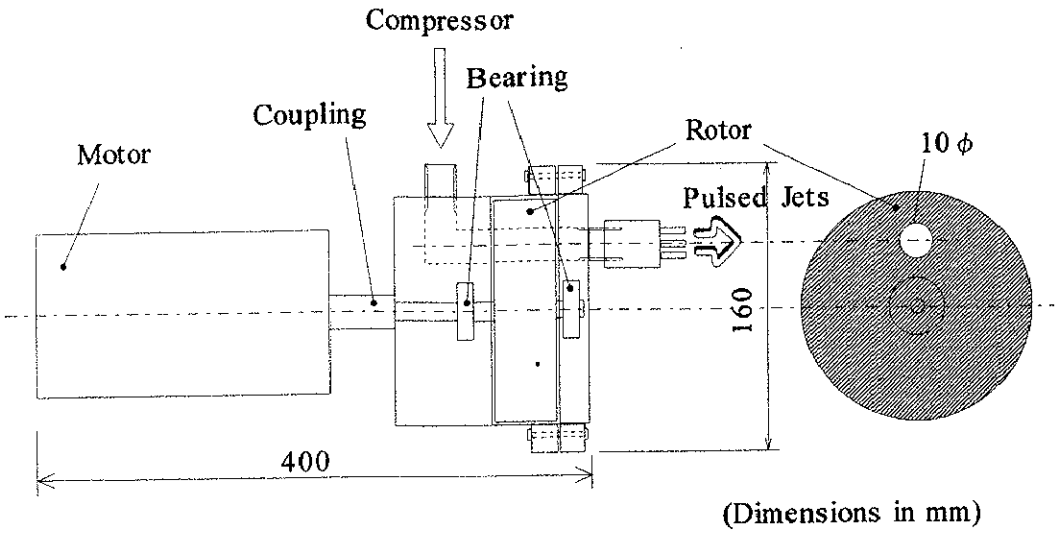

Figure 3.13 Vortex generator jet device.

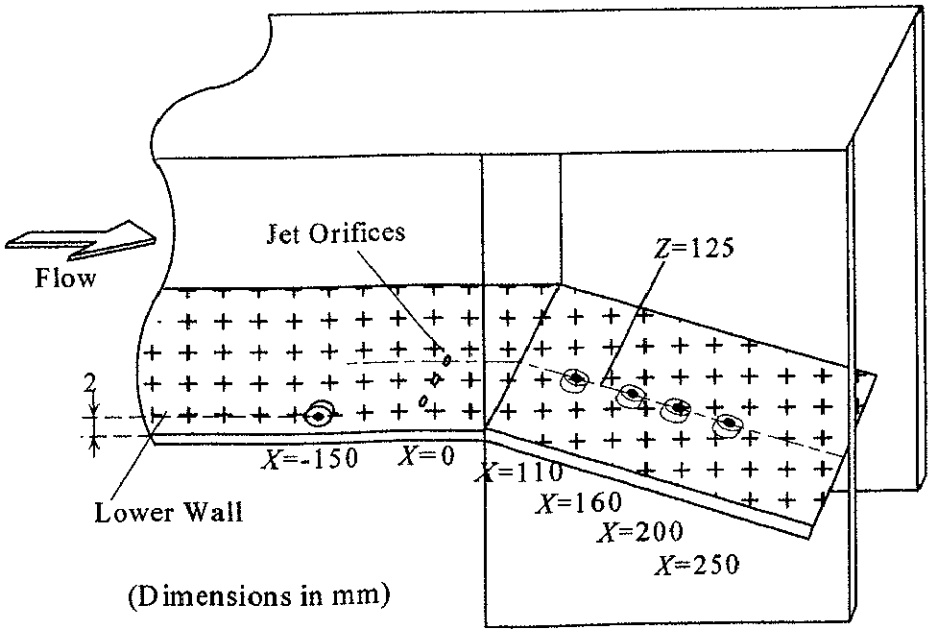

Figure 3.14 Location of static pressure holes in test section.